Effect of Switching the Length of Alkyl Chains on Electric Double Layer Structure and Differential Capacitance at the Electrode Interface of Quaternary Ammonium-Based Ionic Liquids Studied Using Molecular Dynamics Simulation

Seiji Katakura,[†] Naoya Nishi,*,[†] Kazuya Kobayashi,[†] Ken-ichi Amano,[†,‡] and Tetsuo Sakka[†]

[†]Department of Energy and Hydrocarbon Chemistry, Graduate School of Engineering, Kyoto University, Kyoto 615–8510, Japan

[‡]Facluty of Agriculture, Meijo University, Nagoya, Aichi 468–8502, Japan.

E-mail: nishi.naoya.7e@kyoto-u.ac.jp

Phone: (+81) 75 383 2491. Fax: (+81) 75 383 2490

Abstract

Electric double layer structure at the electrode interface has been studied by using molecular dynamics simulation on four quaternary ammonium-based ionic liquids (QaILs) to investigate the effect of switching the alkyl chain length of the Qa cation. These four QaILs are composed of a common anion, bis(trifluoromethanesulfonyl)-amide (TFSA$^-$) and different cations: butyltrimethylammonium (N$_{1114}^+$, $k = 1$), dibutyldimethylammonium (N$_{1144}^+$, $k = 2$), tributylmethylammonium (N$_{1444}^+$, $k = 3$), and tetrabutylammonium (N$_{4444}^+$, $k = 4$), where k represents the number of butyl chains. The difference in k affects the potential dependence for the composition of the first ionic layer and the orientation of butyl chains in the layer. For the case of $k = 1, 2, 3$, the butyl chains parallel to the interface increases as the potential becomes negative, but further negative potential results in the increase in perpendicular ones. In the case of $k = 1$, all the cations in the first ionic layer show the perpendicular orientation at the negative potentials, forming a honeycomb lattice consisting of only cations. On the other hand, in the case of $k = 4$, no change in orientation has been observed due to the geometrical restrictions. The difference in k also affects the differential capacitance. The potential dependence of differential capacitance shows bell shape for the smaller two ($k = 1, 2$) and camel shape for the larger two ($k = 3, 4$). The camel shape for larger IL cations agrees with the prediction from the mean-field lattice gas model and recent experimental results. The differential capacitance at negative potentials deviated to the values higher than the model prediction and the discrepancy becomes greater for smaller k. The results indicate that the potential dependence of ionic orientation significantly affects the differential capacitance. Even for $k = 4$, which does not show the orientational change, the discrepancy has been observed, indicating that not only the orientational change but also the densification of ions in the first ionic layer are the factors we should take into account beyond the lattice gas model.

Introduction

Ionic liquids (ILs) exhibit characteristic liquid structures near the electrified interfaces.[1,2] One of the features of the interfacial structure of ILs is multilayering in which cations and anions show damped oscillation in their density distributions. The formation of the ionic multilayers is a common phenomenon not limited to at the solid and/or electrified interface. The existence of the ionic multilayer structure has also been shown at the interfaces between gas and ILs.[3,4] At the solid interface of ILs, the ionic multilayer structure has been revealed by an atomic force microscopy (AFM).[5–8] When the solid substrate is highly charged, the ionic multilayers consist of alternating layers of cations and anions as found by molecular dynamics (MD) simulations,[9,10] theories,[11,12] and X-ray reflectometry.[10,13] Using MD simulation, Ivaništšev *et al.* showed[9,10] that the density oscillation of alternating layers increases as the electric double layer (EDL) is charged up, but a further charge up causes the attenuation of the oscillation. At the potential where the first ionic layer is eventually saturated with cations or anions, a Helmholtz-like EDL is formed. At potentials with higher charge-up condition from the monolayer state, alternately charged layers form over the first layer. The formation of the alternating layers is called "overscreenin", and the saturation of the first layer is called "crowding".[14]

Differential capacitance (C_d) is an important physical quantity characterizing the EDL structure in an IL. C_d is a macroscopic measurable quantity and reflects the EDL structure at each potential. Therefore, theory and experiment can be directly compared by C_d. C_d is also important in practical use because it is the origin of the capacity (integral capacitance) of electric double layer capacitors. C_d for ILs is known to exhibit potential dependence of bell or camel shape. Such C_d behavior is beyond the electric double layer model of the conventional dilute electrolyte solution system, such as the Gouy-Chapman model.[15,16] Kornyshev proposed a mean field lattice gas model[17] in order to take account of the excluded volume effect between neighboring ions and suggested that this behavior is due to finite volumes of ions. This model has been improved in recent years by adding the effect of

the difference in the size of cation and anion,[18,19] and the contribution of local interaction between ions.[20]

Many studies have been performed on imidazolium-based ILs to clarify the EDL structure of ILs[10,21–34] at the molecular level, but the numbers of studies on quaternary ammonium-based ILs (QaILs), both experimental[35–38] and computational,[39–41] are limited. QaILs have a wide potential window,[42] and therefore are suitable for electrochemical applications.[43] Also, Qa cations have four alkyl groups, and therefore have more degree of freedom to design the IL cation, which would be favorable for fine tunings of interfacial properties. However, the effect of the structure of the Qa cation has not been clarified, while pyrrolidinium-based ILs, which have quaternary ammonium part in their cyclic skeleton, have been studied with several different long and branched side chains.[44,45]

We have studied the structure and dynamics of the EDL of QaILs by using electro-chemical surface plasmon resonance,[35,38] X-ray reflectometry,[36] surface enhanced infrared spectroscopy,[37] and MD simulation.[41] In the MD study on the tributylmethylammonium bis-(trifluoromethanesulfonyl)amide ($[N^+_{1444}][TFSA^-]$),[41] the potential dependence of C_d around the potential of zero charge was reproduced by the EDL model by Kornyshev et al.[17,20] However, the model was not able to reproduce the C_d behavior at negative potentials, where the contribution of the cation is dominant. This discrepancy is due to the change in the orientation of the cation, which is not taken into account in the models,[17,20] suggesting that the orientational preference is another important factor to fully understand the potential dependence of C_d. In our another study on QaILs at the IL|vacuum interface by using MD simulations,[46] we have revealed that the orientational preference of Qa cation depends greatly on the number of its long-chain alkyl groups (k). The orientation of the Qa cation at the electrode interface is also expected to depend on k strongly and to affect the potential dependence of C_d. In the present study, we have studied the EDL structure of four QaILs which have a different number of butyl chains. Clear systematic changes in the EDL structure have been observed with respect to k.

Methods

Computational detail

MD simulation at the interface between four QaILs and graphene electrode was performed using DL_POLY[47] classic. Details of the methodology were described in our previous studies.[41,46] As a common anion for all the QaILs, TFSA$^-$ was used. The cations of QaILs are butyltrimethylammonium (N_{1114}^+, $k = 1$), dibutyldimethylammonium (N_{1144}^+, $k = 2$), N_{1444}^+ ($k = 3$), and tetrabutylammonium (N_{4444}^+, $k = 4$). The structures of these QaILs are shown in Fig. 1. We used CL&P[48] as the force field of QaILs. The version of CL&P used is the same as that in our previous study for the QaIL|vacuum interface.[46] For the force field of graphene, we used the van der Waals parameter of the sp2 carbon atom of OPLS AA.[49] To consider the contribution of mean electronic polarization[50–52] in non-polarized MD simulation, we set relative permittivity $\varepsilon_r = 2$. The value was determined by considering that the refractive index n of these QaILs in the visible light region is about 1.4,[53,54] and the relationship between n and ε_r.

The initial configurations of the QaIL|graphene interface for MD were made in the same way as our previous study on the $[N_{1444}^+][TFSA^-]$|graphene interface.[41] An IL layer was sandwiched between two graphene electrodes, and the distance between the electrodes was fixed to those summarized in Table 1 so that the densities of the ILs at the bulk region ($\pm$ 20 Å from the center for IL) reproduce those obtained from the MD simulation for the ILs|vacuum interface.[46] The mass densities at the bulk region are also summarized in Table 1. Each graphene layer consists of 1008 carbon atoms and the size is (l_x, l_y) = (51.6852 Å, 51.1560 Å). The length of the MD cell in the direction perpendicular to the interface (z-direction) is 300 Å for all the simulations.

The equilibrium structure at the non-charged interface prepared by the above method was used as the initial configuration for all the other potentials. The constant charge method was applied to simulate the charged interface, i.e. the positive and negative charges were
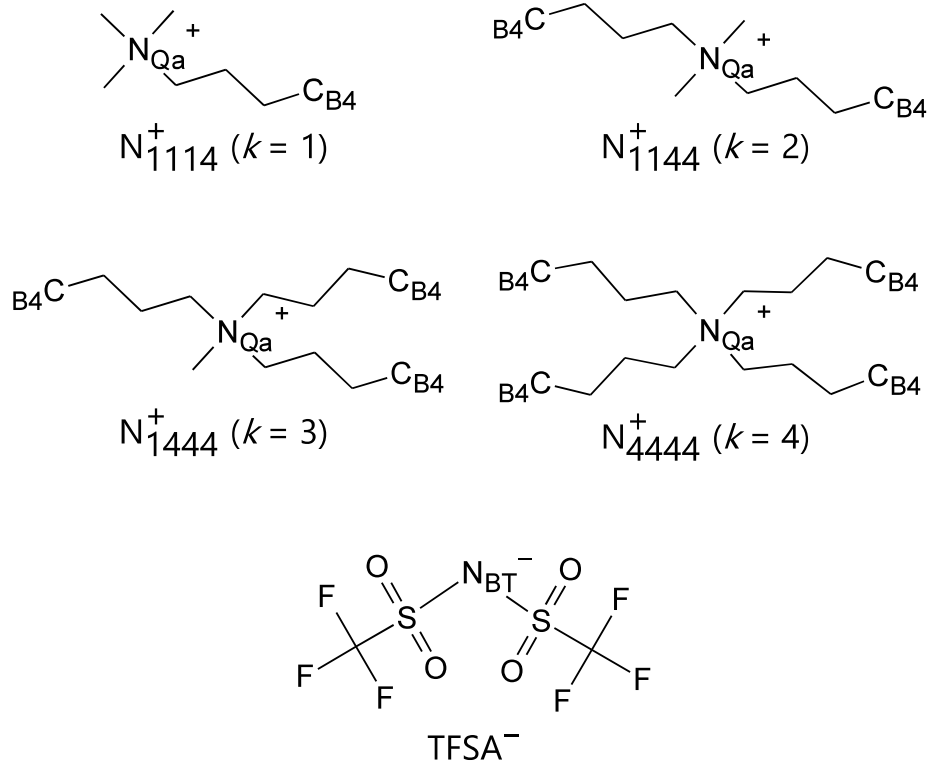
Figure 1: Structures of QaILs and atom names used in the present study.

Table 1: Number of IL ions and distance between two electrodes in the MD cells.

QaIL	number of ion pairs	number of IL atoms	distance between electrodes / Å	Mass density at IL bulk region / $\mathrm{g\,cm^{-3}}$
$[\mathrm{N_{1114}^+}][\mathrm{TFSA^-}]$	560	22960	117.2	1.22
$[\mathrm{N_{1144}^+}][\mathrm{TFSA^-}]$	460	23000	114.1	1.14
$[\mathrm{N_{1444}^+}][\mathrm{TFSA^-}]$	360	21240	103.1	1.09
$[\mathrm{N_{4444}^+}][\mathrm{TFSA^-}]$	340	23120	110.7	1.04

given to the electrodes by evenly allocating the charges to the electrode atoms. The MD simulation was performed for 1 ns to equilibrate, followed by the calculation for 2 ns to produce the trajectory for the data analyses (see Fig. S1). The electric charge was equally allocated to each carbon atom of graphene. The time step was 2 fs. The MD simulation was performed in the NVT ensemble, with controlling the temperature to be 423 K using Berendsen thermostat.[55] The vdW force cut off was $10\,\text{Å}$. Electrostatic interaction was calculated using smooth particle mesh Ewald method (SPME)[56] with an accuracy of 1×10^{-5}. The cutoff distance of SPME is $10\,\text{Å}$. No slab correction was applied for the 3-dimensional SPME. According to our previous study comparing the conditions with and without the correction, the potential was found to be overestimated only by a few percents.[41]

Data analysis

Data analysis was performed in the same way as our previous study on $[\text{N}_{1444}^{+}][\text{TFSA}^{-}]$.[41] As in the previous study, we focused on the N atoms of the Qa cations and TFSA^{-} anions and the C atom at the terminal of the butyl chain. We refer them as N_{Qa}, N_{BT}, and C_{B4}, respectively (Fig. 1).

From the MD trajectories, the number density distribution $\rho_{\text{num,i}}$ of each atom i and the charge density distribution ρ_{chg} were analyzed. The ρ_{chg} profile was integrated by one-dimensional Poisson equation to calculate the potential profile ϕ in the z-direction. The interfacial potential difference $\Delta\phi$ was defined as the potential at the electrode ϕ_{elec} with respect to that at the ionic liquid bulk ϕ_{bulk}, i.e., $\Delta\phi = \phi_{\text{elec}} - \phi_{\text{bulk}}$. In the following, $\Delta\phi$ is simply referred to as the interfacial potential difference.

Based on the first peak of $\rho_{\text{num,NQa}}$ at all potentials, the range of the first ionic layer formed by the cation was determined to be $z = 0\,\text{Å}$ to $6.55\,\text{Å}$ for $k = 1, 2, 3$, and $z = 0\,\text{Å}$ to $5.65\,\text{Å}$ for $k = 4$ with the z-axis defined as $z = 0\,\text{Å}$ at the graphene position and $z > 0\,\text{Å}$ for the IL phase. Similarly, the range of the first anionic layer was determined based on $\rho_{\text{num,NBT}}$ to be $z = 0\,\text{Å}$ to $6.95\,\text{Å}$ for all k. For the non-polar moiety of the Qa cation, the range was

$z = 0\,\text{Å}$ to $6.45\,\text{Å}$ for all k. Note that when a C_{B4} atom is in the first layer, the C_{B4} atom is counted as belonging to the first ionic layer even if the N_{Qa} covalently connecting to the C_{B4} atom is located at the second layer.

Orientations were analyzed for the butyl chains. N_{Qa} atoms present in the first ionic layer were selected, and the N_{Qa}-C_{B4} intramolecular vectors were analyzed for all the butyl chains connected to the N_{Qa}. Regarding the angle θ formed by the intramolecular vector and the z-axis, the orientational distribution function $p(\theta)$ was analyzed. The $p(\theta)$ is defined by the following equation.[41,46]

$$\int_0^\pi \frac{p(\theta)}{2} \sin\theta\mathrm{d}\theta = 1 \tag{1}$$

In this equation, isotropy is assumed for the azimuth angle. $p(\theta)$ represents the relative probability of the orientation at θ with respect to isotropic orientation. In other words, $p(\theta)/2$ and $(p(\theta)\sin\theta)/2$ are probability density functions in terms of the solid angle and θ, respectively. When the intramolecular vector is isotropically oriented about θ, $p(\theta)$ is unity at all θ.

The surface charge density of the electrode (σ_{elec}) was differentiated with respect to the potential, and the differential capacitance (C_{d}) was calculated from the slope. This numerical differentiation was performed by fitting a quadratic expression to five consecutive points. At the same time, the standard error was also calculated. The data points around 0 V in the C_{d}-$\Delta\phi$ plot, where N_{Qa} and N_{BT} co-exist in the first ionic layer, were fitted with the theoretical formula of C_{d} by the lattice gas model proposed by Kornyshev $et~al.$[17,20] as follows.

$$C_{\text{d}} = C_{\text{d0}} \frac{\cosh\left(\alpha u/2\right)}{1 + 2\gamma\sinh^2\left(\alpha u/2\right)} \sqrt{\frac{2\gamma\sinh^2\left(\alpha u/2\right)}{\ln\left(1 + 2\gamma\sinh^2\left(\alpha u/2\right)\right)}} \tag{2}$$

where C_{d0} is C_{d} at 0 V, u is the reduced potential $u = e\Delta\phi/k_{\text{B}}T$, α is a parameter expressing short-range interaction between ions. The parameter γ is defined as the fraction of occupied

lattice in the bulk and could also be expressed as follows.

$$\gamma = 2C_{\text{bulk}}/C_{\text{max}} \tag{3}$$

where C_{bulk} is the ion concentration at bulk and C_{max} is the maximal local concentration of the ion. Given that γ takes different values for cations and anions ($\gamma_+ \neq \gamma_-$), the following potential dependence of γ may be assumed.[17]

$$\gamma = \gamma_- + \frac{\gamma_+ - \gamma_-}{1 + \exp{(\alpha u)}} \tag{4}$$

Among the parameters in the above equations, γ_+, γ_-, α, and C_{d0} were used as fitting parameters.

Results and Discussions

Number density distributions

The contour maps of the normalized number density distributions of N_{Qa} and N_{BT} as a function of z and potential are shown in Figs. S2 and S3, respectively. There is no significant difference in the number density distributions among the four QaILs. In contrast the contour maps for C_{B4} atoms, shown in Fig. 2, show the strong k dependence.

First of all, we focus on the features commonly found in the first peak of all the QaILs. QaILs showed the first layer peak at about $4\,\text{Å}$. The position does not depend on the number of butyl chains because the first layer peak comes from the butyl chain in contact with graphene. This first layer peak almost disappeared at potentials more positive than the same threshold potential (~ 3 V) for all the QaILs. The disappearance of the first layer peak means that the first layer becomes solely composed of TFSA$^-$. The same threshold potential for all the QaILs implies that the structure of the first ionic layer and even C_{d} are not significantly influenced by the number of butyl chains of the cation at positive potentials
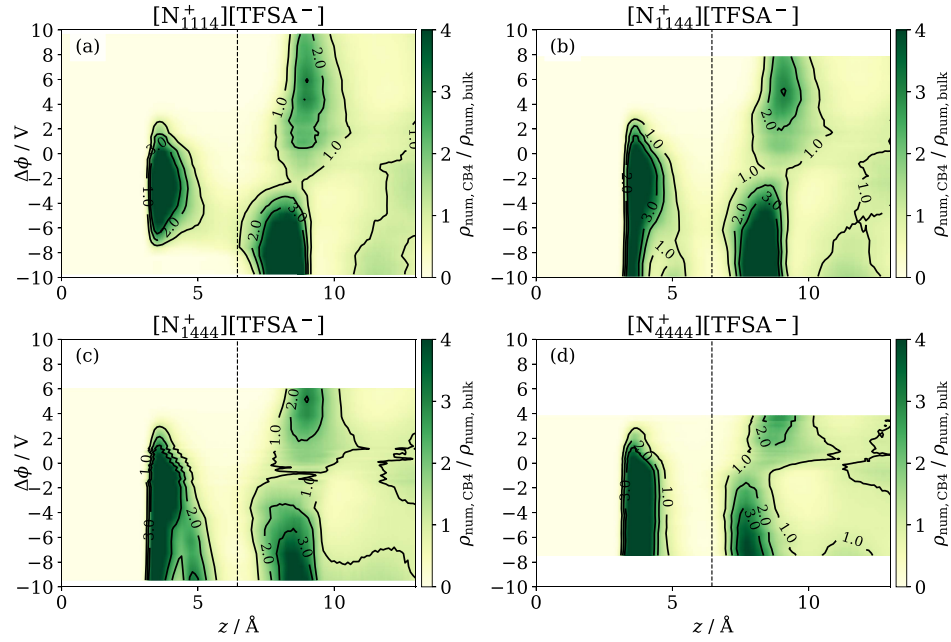
9

Figure 2: Contour maps of the normalized number density of C_{B4} on z-$\Delta\phi$ plane. The vertical dotted lines are the schematic boundary between the first and second layers.
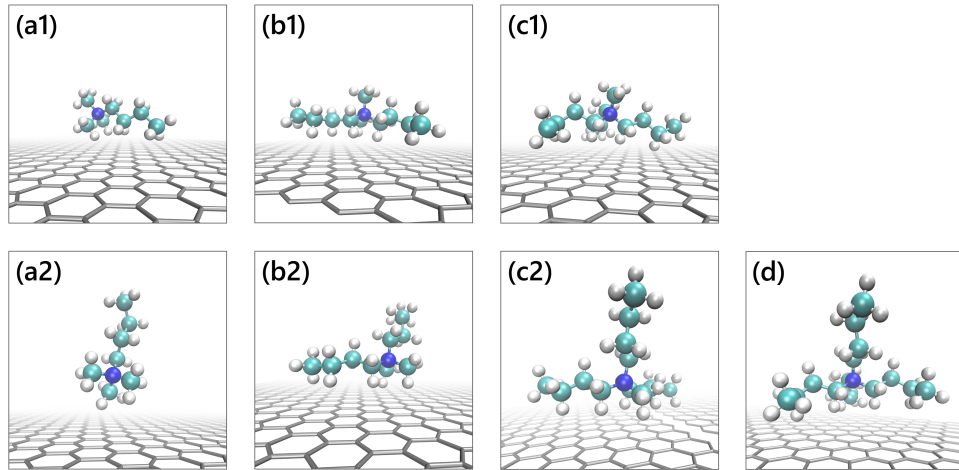

Figure 3: Snapshots of N_{1114}^+ (a), N_{1144}^+ (b), N_{1444}^+ (c), and N_{4444}^+ (d) in the first ionic layer viewed from the lateral direction. (1) Lying orientation in which all the butyl chain parallel to the electrode. (2) Standing orientation in which one or more butyl chains pointing to the IL bulk. N_{4444}^+ shows the standing orientation only.

(> 3 V), as we will see in the later section.

On the other hand, the first peak behavior at the negative potentials depends on the QaILs, which includes the increase, decrease, and disappearance of the peak. A particularly distinctive difference is that the first peak disappeared below -8 V only when $k = 1$. Therefore, we will first focus on the behavior of $k = 1$, in detail (Fig. 2(a)). The height of the first peak has a maximum at -2 V and disappears at -8 V. This behavior can be explained by the change in the fraction of two kinds of orientations of N_{1114}^+ as shown in Fig. 3(a). In the vicinity of 0 V, N_{1114}^+ takes both the two orientations in which the butyl chain stands (standing orientation, Fig. 3(a2)) and lies (lying orientation, Fig. 3(a1)). In the definition of the present study (see Data analysis section), the C_{B4} of N_{1114}^+ in the standing orientation corresponds to the second peak in Fig. 2 and that in the lying orientation corresponds to the first peak. Therefore, the behavior of the first peak shown in Fig. 2 indicates that the fraction of N_{1114}^+ in the lying orientation increases as the potential becomes more negative, and reaches a maximum at -2 V and at further negative potentials the fraction decreases. At the potentials below -8 V the fraction reaches zero, which means that all the N_{1114}^+ at the first ionic layer are in the standing orientation.

The behavior for $k = 2$ (Fig. 2(b)) and 3 (Fig. 2(c)) was consistent with $k = 1$ in terms of the increase in the lying orientation at negative potentials and the increase in the standing orientation at further negative potentials. However, different behavior was also found; the splitting of the first peak is observed for $k = 2$ and 3, and the attenuation of the peak was not observed for $k = 3$. For $k = 4$, the first peak did not show a characteristic change in the height and shift at all, suggesting that N_{4444}^+ does not show orientational change at negative potentials. In the later section, we will describe the result of more direct analysis in the orientation.

For $k = 2$ or 3, the first peak did not disappear even at more negative potentials than ~ -8 V, unlike $k = 1$. This comes from the difference in the standing orientation. For example, in the standing orientation of N_{1144}^+, one butyl chain stands but the other lies. Of

11

course, there are some N_{1144}^+ ions with both the two butyl chains standing, but they are in a minority. Due to the one-butyl-lying orientation, C_{B4} continues to remain at the first layer even at very negative potentials.

Composition of first ionic layer

The surface density Γ_i of N_{Qa}, N_{BT}, and, C_{B4} present in the first layer region are shown in Fig. 4. These Γ_i represent the dependence of the QaILs composition in the first layer.
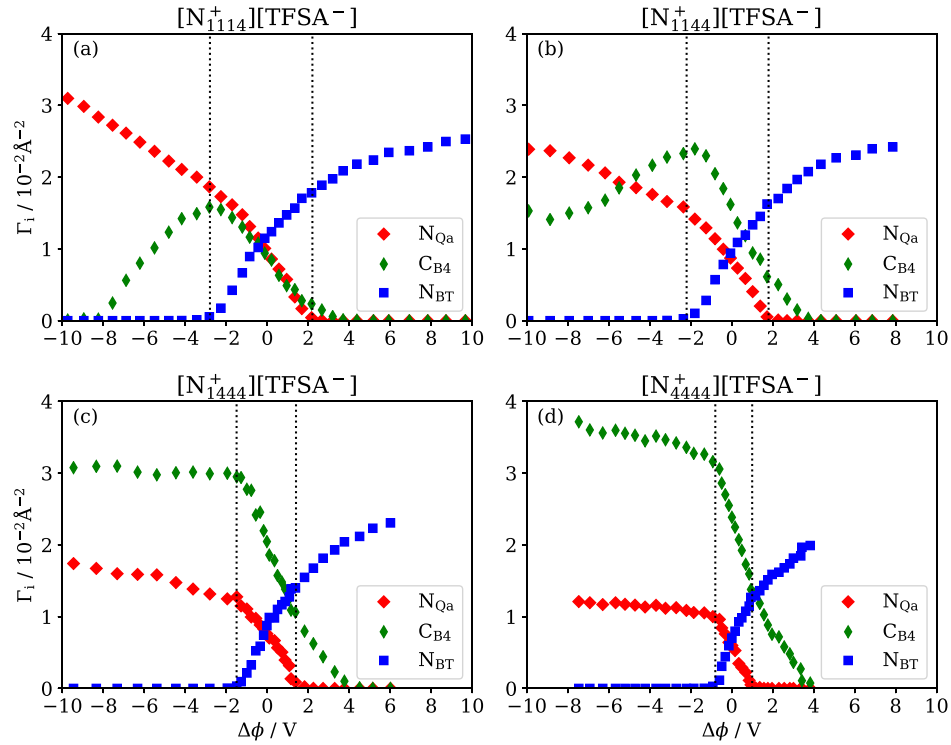

Figure 4: Surface density of N_{Qa} (red), N_{BT} (blue), C_{B4} (green) at the first layer. The boarder between the first and second layer (z_{div}) for N_{Qa}, N_{BT}, C_{B4} are shown in Figs. S2, S3, 2, respectively.

As expected, Γ_{NQa} increased at more negative potentials and Γ_{NBT} increased at more positive potentials. There was no significant difference in Γ_{NBT} for the four QaILs. Also, the potential at which Γ_{CB4} is depleted on the positive potential side also agreed for all the QaILs ($\sim 4\,\mathrm{V}$). This is because the Qa cations hardly contribute to the potential screening

at potentials where the first layer is constituted only by TFSA$^-$, as described above.

On the other hand, the behavior of Γ_{NQa} and especially Γ_{CB4} varied with the QaILs. From our previous study in the case of $k = 3$,[41] we know that the behaviors of Γ_{NQa} and Γ_{CB4} are roughly divided into three potential regions. Among the four QaILs, $k = 3$ clearly showed the difference between these potential regions. Hence, in the following, using Fig. 4(c) as an example, we will explain the behavior of Γ_{NQa} and Γ_{CB4} of QaILs for each of these three potential regions.

In the first potential region cations and anions coexist in the first layer. In Fig. 4(c) the region corresponds to $-1.5\,\mathrm{V}$ to $1.5\,\mathrm{V}$. Here we call this potential region the coexistence region. In this coexistence region, Γ_{NQa} increases at negative potentials, and the slope is the steepest compared with the other potential regions. The coexistence region around 0 V becomes narrow with increasing k. Simultaneously, the increase in k causes more enhanced exchange (steeper slope) of TFSA$^-$ and polar portion and butyl chains of Qa cation. Focusing on Γ_{CB4} at the negative boundary of the coexistence region, clearly Γ_{CB4} is larger for greater k, indicating that the fraction of butyl chain in the first layer is higher for greater k.

The second potential region is at potentials more negative than the coexistence region, where the TFSA$^-$ is completely depleted from the first layer, and the polar part of the cation competes with the non-polar part. In Fig. 4(c), this part corresponds to $-6\,\mathrm{V}$ to $-1.5\,\mathrm{V}$. Here, we call this potential region the condensing region. In the condensing region, the Qa cation in the first layer increases the local concentration and the fraction of the standing orientation as the potential becomes negative. The high concentration can be achieved because the occupation area per cation on the electrode is smaller in the standing orientation than the lying orientation. Due to this difference in the electrode occupation area, Γ_{NQa} can increase even though the anion is completely depleted from the first layer.

For the four QaILs, the behaviors of Γ_{NQa} and Γ_{CB4} in the condensing region were significantly different. For $k = 1$ (Fig. 4(a)), Γ_{CB4} decreased as the potential becomes more negative and it becomes negligible at $-8\,\mathrm{V}$. This means that all N$_{1114}^+$ ions have become in

the standing orientation. Γ_{NQa} increased as the potential become even more negative than $-8\,\text{V}$. This condensation is due to the rearrangement of N_{1114}^{+} into more dense structure. For $k = 2$ (Fig. 4(b)), Γ_{CB4} decreased as the potential become more negative but converged to a finite value $\sim 1.5 \times 10^{-2}\,\text{Å}^{-2}$ unlike the case with $k = 1$. The decrease indicates the standing orientation increased, the same as for $k = 1$. The convergence to a non-zero value is specific to cations with multiple alkyl chains ($k \geq 2$); some butyl chains remain in the first layer even in the standing orientation. For $k = 3$ ((Fig. 4(c)), Γ_{CB4} was almost constant in the condensing region regardless of the potential. Like $k = 2$, this results from the balance between the two effects. For $k = 4$ ((Fig. 4(d)), both Γ_{NQa} and Γ_{CB4} increased as the potential becomes more negative. However, the rate of increase of Γ_{NQa} was significantly small compared to the other QaILs. As shown in the later section, the orientation of N_{4444}^{+} is almost independent of the potential. Therefore, the increase in Γ_{NQa} and Γ_{CB4} are not due to the change in the orientation of N_{4444}^{+}, but are due to the densification of N_{4444}^{+}. Such an effect also appeared clearly for $k = 1$ as already mentioned. Even in the cases with $k = 2$, 3, the same effect seems to exist although it is not as clear as with $k = 1$, 4.

In the third potential region, the fraction of the Qa cation in the standing orientation can no longer increase any more, and Γ_{NQa} is almost saturated. It corresponds to $-6\,\text{V}$ or more negative in Fig. 4(c). Here, we call this potential region the crowding region. In the crowding region, charging of the EDL occurs by the accumulation of cations in the second layer because the first layer is already saturated with cations. Such a phenomenon has already been found in previous studies by MD[9,57] and theory[11,12,17] as "ion crowding". For k = 2, 3, and 4, small kinks were observed for Γ_{NQa} at -9, -5, and $-4\,\text{V}$, where the crowding occurred judged from the appearance of the second peak in the number density distribution of N_{Qa} (Fig. S2). On the other hand, when $k = 1$, the crowding region was not observed. The potential at which the crowding occurs for $k = 2$, 3, and 4 negatively shifts as k decreases. Hence, the crowding is expected to occur in the case of $k = 1$ at more negative potentials beyond the potential range investigated.

Fig. 5 shows the snapshots of the first layer at the most negative potentials investigated and therefore in the crowding region. For the case with $k = 2, 3$, and 4, the QaILs did not exhibit well ordered two dimensional structure, but $[N_{1114}^+][TFSA^-]$ exhibit honeycomb lattice. Two dimensional structure has been reported in a MD study on 1-butyl-3-methylimidazolium hexafluorophosphate[58] and in a scanning tunnel microscope study on 1-butyl-1-methylpyrrolidinium tris(pentafluoroethyl)trifluorophosphate.[59] The former reported honeycomb lattice composed of both the cations and anions, and the latter reported linear lattice of cations at negative potential. Unlike these cyclic compounds and the present multi-alkyl Qa ions, N_{1114}^+ has less bulky polar part and more symmetric rod-like structure and therefore the polar parts of the neighboring N_{1114}^+ can be close enough to form honeycomb lattice entirely composed of cations.
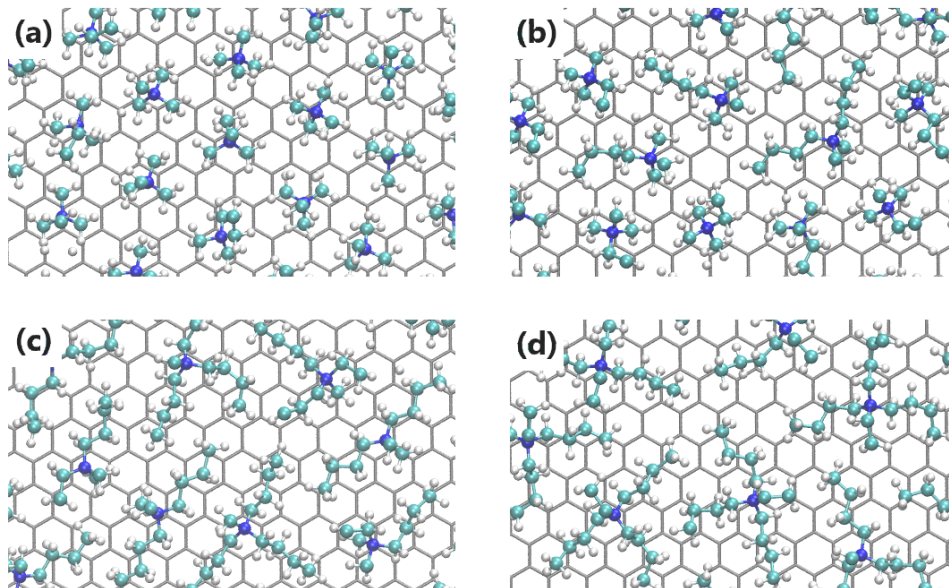

Figure 5: Snapshots of the first layer at the most negative potentials. (a) N_{1114}^+ (b) N_{1144}^+ (c) N_{1444}^+ (d) N_{4444}^+. Butyl chains at the second layer region are not displayed. Only N_{1114}^+ showed hexagonal array.

Orientational distribution of butyl chain in Qa cations

As indicated by the snapshot (Fig. 3) and composition (Fig. 4), the Qa cations in the first layer change their orientation depending on the potential. In order to examine the orientation of Qa cation more directly, the orientational distribution of the butyl chains was analyzed. The orientation distribution function of the butyl chain is shown in Fig. 6.
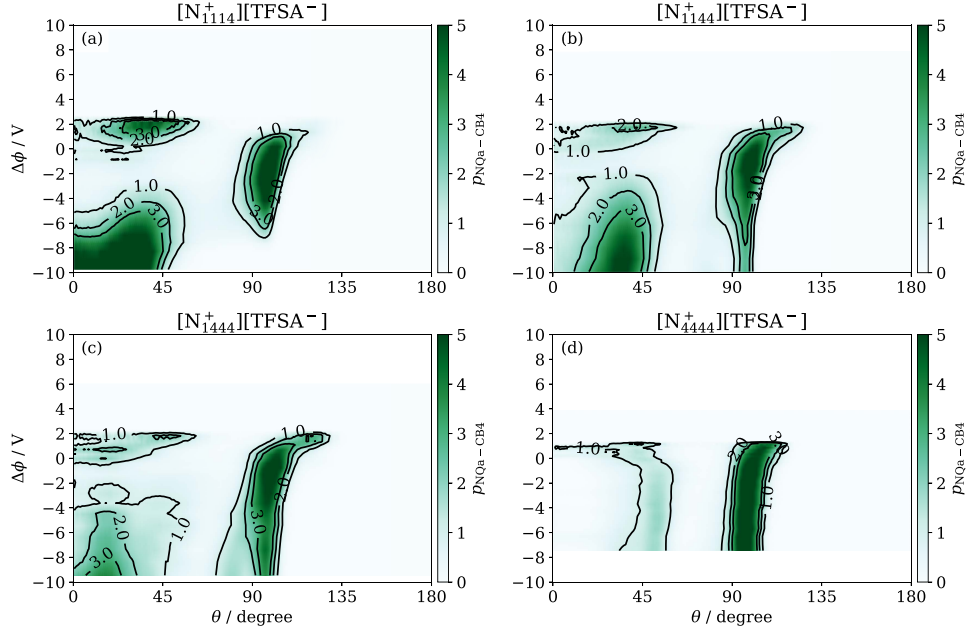
Figure 6: Contour maps of orientational distribution $p_{\mathrm{NQa-CB4}}$ on the θ-$\Delta\phi$ plane, where θ = 0° represents that the butyl chain point to the IL bulk phase and θ = 90° represents that the butyl chain is parallel to the electrode.

Among all the QaILs, a sharp peak near 90 degrees and a broad peak from 0 to 60 degrees were observed. The presence of the former and latter peaks indicates that the butyl chains are parallel and perpendicular to the interface, respectively. Note that the sharp peak has contributions from both the standing and lying orientations of the Qa cation except for k = 1 (Fig. 3). This is because, in the case with $k \geq 2$, some butyl chains are lying even if the Qa cation takes the standing orientation (Fig. 3(b2), (c2), and (d)). Nevertheless, the sharp and broad peaks mainly reflect the lying and standing orientations, respectively. For k = 1, 2, 3, the sharp peak was highest around $-2\,\mathrm{V}$. On the other hand, the broad peak increased

as the potential becomes more negative than $-2\,\mathrm{V}$. However, for $k = 4$, the orientation of N_{4444}^{+} hardly changed, which agrees with the number density distribution (Fig. 2(d)) and first layer composition (Fig. 4(d)).

In order to more directly investigate the potential dependence of orientation, the distribution function of orientation was integrated based on Eq. (1) to calculate the fraction of the two orientations. The fraction as a function of potential is shown in Fig. 7. The results were significantly different between $k = 1$, 2, 3, and $k = 4$. Focusing on the proportion of standing butyl chain (purple plots), local minima were found at -2, -1.5, and $-1\,\mathrm{V}$ for k = 1, 2, and 3, respectively. These minima show that the Qa cations in the lying orientation increase as the potential becomes more negative than $0\,\mathrm{V}$, but the standing orientation increases at further negative potentials. The potentials at the minima correspond roughly to the potentials where Γ_{NBT} becomes 0 in Fig. 4. Also, in the case of $k = 2$, 3, the fractions converged to constant values at negative potentials. These different behaviors occurred at the coexistence, condensing, and, crowding regions, respectively. On the other hand, for k = 4, the orientation fractions showed constant values at almost all potentials. The fraction of standing butyl chain was 0.25, which indicates that no orientation change occurs from the state where only one of the four butyl chains in N_{4444}^{+} stands.

Differential capacitance

The potential dependence of C_{d} of the four QaILs is shown in Fig. 8, and the best fit curves of the lattice gas model proposed by Kornyshev et al.[17,20] are shown in Fig. 9. The fitting parameters are shown in Table 2. Regardless of the difference in cation size, the four QaILs showed almost the same C_{d} around 0 V. In terms of the Debye length, the smaller ion gives the larger C_{d} because of the increase in the bulk ionic density. The contradiction between the Debye length and the present simulation results suggests that the estimation with the Debye length is invalid in ILs. The reason is ascribed to the Debye length (1 Å) smaller than the ion size (10 Å), which apparently contradicts the point-charge assumption. Because of
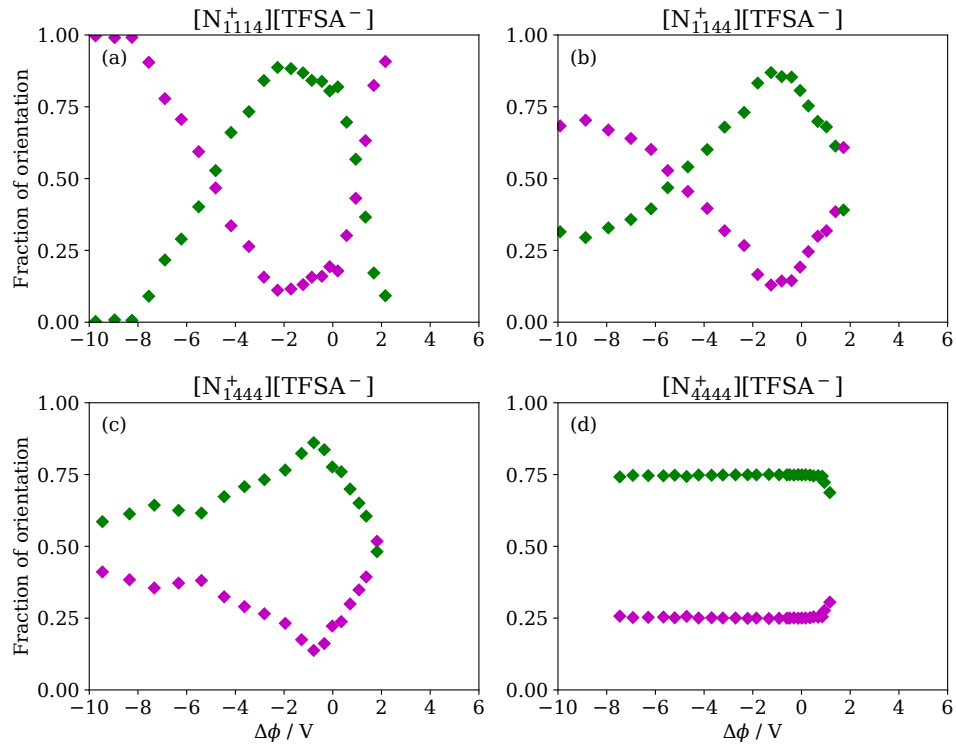
Figure 7: Fraction of butyl chain pointing to the IL bulk phase (purple) and parallel to the electrode (green). The fraction was calculated based on the integration in Eq. (1).

the excluded volume of the ions, the first ionic layer almost determines C_d near 0 V like in the Stern model (or the Helmholtz model), and therefore the distance between the "surface" ion and the electrode is the most important determinant. The only small difference in C_d around 0 V is due to the similar distances among the four QaILs as shown in Figs. 3, S2, and S3.

Table 2: Best fit parameters of the fitting of the theoretical equation (Eq. (2)) of lattice gas model[20] to the C_d-$\Delta\phi$ plots (Fig. 9).

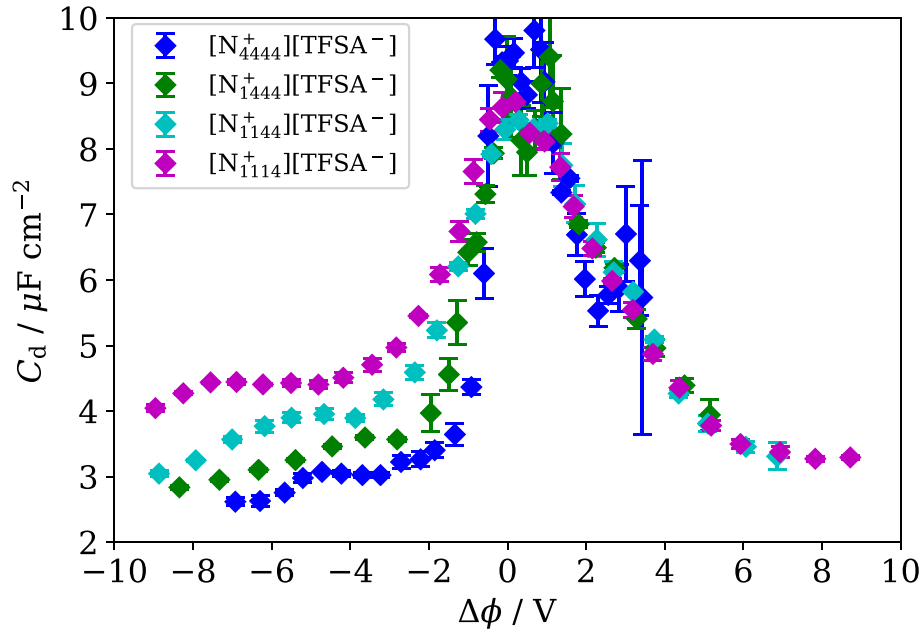| Qa cation	Range of $\Delta\phi$ for fitting / V	C_{d0} / μF cm^{-2}	γ_+	γ_-	α
N_{1114}^+	−2.8 to 2.2	8.6 ± 0.1	0.6 ± 0.2	0.40 ± 0.08	0.05 ± 0.01
N_{1144}^+	−1.8 to 1.7	8.3 ± 0.1	0.46 ± 0.05	0.25 ± 0.02	0.085 ± 0.008
N_{1444}^+	−1.5 to 1.4	8.7 ± 0.2	0.7 ± 0.2	0.23 ± 0.02	0.08 ± 0.02
N_{4444}^+	−0.9 to 1.2	9.6 ± 0.4	0.8 ± 0.3	0.25 ± 0.04	0.1 ± 0.05

Figure 8: Potential dependence of differential capacitance.

The C_d-$\Delta\phi$ plots exhibited bell-shape and camel-shape behavior in the cases of $k = 1$, 2, and 3, 4, respectively. The transition from bell-shaped to camel-shaped behavior with increasing the ionic size agrees with the prediction from the mean-field lattice gas model[17] and our previous experimental study for C_d measurement.[60] The best-fitted ion
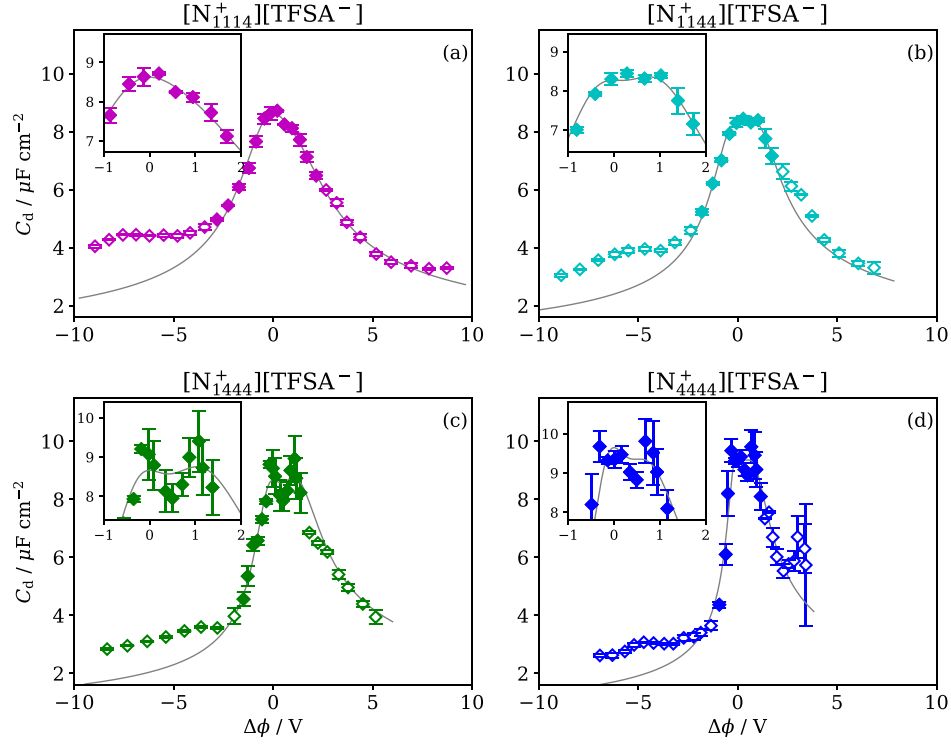
Figure 9: Potential dependence of differential capacitance and the theoretical curve (gray line) of Eq. (2) fitted to the data near $\Delta\phi = 0$ (solid diamond). .

interaction parameter α was smaller for smaller k. α is a parameter reflecting local inter-ionic interactions; it decreases from unity with increasing the relative strength of like-ion repulsion against unlike-ion attraction.[20] The smaller α for smaller k is presumably ascribable to the stronger repulsion between cations due to smaller ionic size, while the attraction between neighboring cation and anion is rather similar irrespective to k because the polar part of the cation can be close to the anion. It should be noted that the value of α depends on the MD method. In a previous MD study[61] using a spherical model, Haskins and Lawson compared the constant charge method (constant-σ), which we used in the present study, and the constant potential method (constant-$\Delta\phi$). They showed that the C_{d}-$\Delta\phi$ plots for the latter method have a shallower slope and smaller α because of the weakened electrostatic interaction between the electrode and ions by the induced dipoles. The same tendencies were also reported by the MD simulations[25,31,62] using all-atom models. Although a further study is necessary to compare MD simulation with the lattice gas model, it is still meaningful to discuss the order of α values for different k in the present study.

The C_{d} values at negative potentials decreased as k increased, indicating that the larger k leads to the suppression of cation concentration rise in the first layer. In spite of the notable difference at negative potentials, there was an only small difference among the QaILs at positive potentials. Since the potential is almost determined by the structure of the first ionic layer, the small difference means that the structure of first ionic layer composed of TFSA$^-$ at positive potentials is not significantly affected by the structure of Qa cation. However, in the case of $k = 4$, there is a difference from the other three cases, suggesting the butyl chains in the TFSA$^-$ layer still affect the layer structure due to relatively high Γ_{CB4} value for $k = 4$.

As in our previous study of [N$_{1444}^+$][TFSA$^-$],[41] the lattice gas model reproduced the C_{d}-$\Delta\phi$ plots by MD, but a discrepancy between the theoretical curve and MD results at negative potentials is clearly discernible (Fig. 9). For all the QaILs, the discrepancy increased in the condensing region. The discrepancy was smaller as k increased, but it even existed at $k =$

4. In the previous study, we considered that the main factor of the discrepancy lies in the orientational change of the Qa cation. However, N^+_{4444} does not have such an orientational change (e.g. Fig. 7(d)). Therefore there seems a factor other than the orientation change of the Qa cation. The densification of ions in the first layer is a presumable reason, which was also observed in our previous experimental studies.[36,60,63] In a lattice gas model, such densification corresponds to an increase in the lattice sites and decrease in γ. Such an effect is not included in the lattice gas models, which would be the reason why the discrepancy was also seen in symmetrical N^+_{4444}. Nonetheless, the most significant discrepancy at $k = 1$ supports that orientational change is a major factor. Both the densification and orientational change contributes to the higher C_d value than the theoretical curve at negative potentials.

Conclusions

The potential dependence of the electrical double layer structure and differential capacitance at the interface between QaILs and graphene electrode interface were investigated for four types of QaILs by changing the number (k) of butyl chains in the Qa cation.

Surface density of the polar part of Qa cations in the first layer (Γ_{NQa}) revealed that the increase in k (larger cation) causes cation saturation in the first layer at less negative potential. Also, the behavior of the butyl chain (Γ_{CB4}) significantly depended on k.

The orientational analysis of the butyl chain for $k = 1$ and 2 showed that the fraction of lying orientation increases as the potential becomes negative, but then standing orientation increased at further negative potentials, which agrees with the result in a previous study for $[N^+_{1444}][TFSA^-]$ ($k = 3$).[41] However, in the case of N^+_{4444} ($k = 4$), the ratio of butyl chains parallel to the electrode to those vertical was 3:1 at almost all the potentials, which means that the geometry of N^+_{4444} does not allow it to be in the lying orientation. Only $[N^+_{1114}]$ $[TFSA^-]$ exhibited honeycomb lattice at negative potential because of its less-bulky polar part.

C_d around 0 V was almost the same in all the QaILs. The similarity contradicted the C_d difference estimated by Debye length, which means that screening of the electric field generated from the electrodes is almost achieved only in the first layer. At positive potentials, where TFSA$^-$ is dominant in the first layer, the C_d-$\Delta\phi$ plot in all the QaILs was almost the same, while at negative potentials, where Qa cation is dominant, C_d was smaller for larger k. As in the previous study on [N$_{1444}^+$][TFSA$^-$],[41] the theoretical curve of the lattice gas model failed to reproduce the C_d behavior at negative potentials. The change in orientation of the cations is the reason of this deviation as was suggested in the previous study of [N$_{1444}^+$][TFSA$^-$]. However, even N$_{4444}^+$, which is more symmetric and therefore should have little contribution from orientational change, showed the discrepancy, which suggests another contribution, i.e., the densification of the Qa ions more closely packed at more negative potentials.

Acknowledgement

Supporting Information Available

Normalized number densities of N$_{Qa}$ and N$_{BT}$ on z-$\Delta\phi$ plane.

References

(1) Fedorov, M. V.; Kornyshev, A. A. Ionic Liquids at Electrified Interfaces. *Chem. Rev.* **2014**, *114*, 2978–3036.

(2) Hayes, R.; Warr, G. G.; Atkin, R. Structure and Nanostructure in Ionic Liquids. *Chem. Rev.* **2015**, *115*, 6357–426.

(3) Nishi, N.; Yasui, Y.; Uruga, T.; Tanida, H.; Yamada, T.; Nakayama, S.; Matsuoka, H.; Kakiuchi, T. Ionic Multilayers at the Free Surface of an Ionic Liquid, Trioctylmethylammonium Bis(Nonafluorobutanesulfonyl)Amide, Probed by X-Ray Reflectivity Measurements. *J. Chem. Phys.* **2010**, *132*, 164705.

(4) Haddad, J.; Pontoni, D.; Murphy, B. M.; Festersen, S.; Runge, B.; Magnussen, O. M.; Steinrück, H.-G.; Reichert, H.; Ocko, B. M.; Deutsch, M. Surface Structure Evolution in a Homologous Series of Ionic Liquids. *Proc. Natl. Acad. Sci. USA* **2018**, *115*, E1100–E1107.

(5) Atkin, R.; Warr, G. G. Structure in Confined Room-Temperature Ionic Liquids. *J. Phys. Chem. C* **2007**, *111*, 5162–5168.

(6) Li, H.; Wood, R. J.; Endres, F.; Atkin, R. Influence of Alkyl Chain Length and Anion Species on Ionic Liquid Structure at the Graphite Interface as a Function of Applied Potential. *J. Phys. Condens. Matter* **2014**, *26*, 284115.

(7) Yokota, Y.; Hara, H.; Morino, Y.; Bando, K.-i.; Imanishi, A.; Uemura, T.; Takeya, J.; Fukui, K.-i. Molecularly Clean Ionic Liquid/Rubrene Single-Crystal Interfaces Revealed by Frequency Modulation Atomic Force Microscopy. *Phys. Chem. Chem. Phys.* **2015**, *17*, 6794–6800.

(8) Amano, K. I.; Yokota, Y.; Ichii, T.; Yoshida, N.; Nishi, N.; Katakura, S.; Imanishi, A.; Fukui, K. I.; Sakka, T. A Relationship Between the Force Curve Measured by Atomic Force Microscopy in an Ionic Liquid and Its Density Distribution on a Substrate. *Phys. Chem. Chem. Phys.* **2017**, *19*, 30504–30512.

(9) Ivaništšev, V.; Fedorov, M. V. Interfaces between Charged Surfaces and Ionic Liquids: Insights from Molecular Simulations. *Electrochem. Soc. Interface* **2014**, *23*, 65–69.

(10) Uysal, A.; Zhou, H.; Feng, G.; Lee, S. S.; Li, S.; Fenter, P.; Cummings, P. T.; Fulvio, P. F.; Dai, S.; McDonough, J. K. *et al.* Structural Origins of Potential Dependent

Hysteresis at the Electrified Graphene/Ionic Liquid Interface. *J. Phys. Chem. C* **2014**, *118*, 569–574.

(11) Bazant, M. Z.; Storey, B. D.; Kornyshev, A. A. Double Layer in Ionic Liquids: Over-screening Versus Crowding. *Phys. Rev. Lett.* **2011**, *106*, 046102.

(12) Bazant, M. Z.; Storey, B. D.; Kornyshev, A. A. Double Layer in Ionic Liquids: Over-screening Versus Crowding (Vol 106, 046102, 2011). *Phys. Rev. Lett.* **2012**, *109*, 2.

(13) Mezger, M.; Schröder, H.; Reichert, H.; Schramm, S.; Okasinski, J. S.; Schröder, S.; Honkimäki, V.; Deutsch, M.; Ocko, B. M.; Ralston, J. *et al.* Molecular Layering of Fluorinated Ionic Liquids at a Charged Sapphire (0001) Surface. *Science* **2008**, *322*, 424–428.

(14) Ivanistsev, V.; O'Connor, S.; Fedorov, M. V. Poly(a)morphic Portrait of the Electrical Double Layer in Ionic Liquids. *Electrochem. Commun.* **2014**, *48*, 61–64.

(15) Chapman, D. L. LI. A Contribution to the Theory of Electrocapillarity. *Phil. Mag.* **1913**, *25*, 475–481.

(16) Gouy, M. Sur la Constitution de la Charge ÉLectrique à la Surface d'un ÉLectrolyte. *J. Phys. Theor. Appl.* **1910**, *9*, 457–468.

(17) Kornyshev, A. A. Double-Layer in Ionic Liquids: Paradigm Change? *J. Phys. Chem. B* **2007**, *111*, 5545–5557.

(18) Han, Y.; Huang, S.; Yan, T. A Mean-Field Theory on the Differential Capacitance of Asymmetric Ionic Liquid Electrolytes. *J. Phys. Condens. Matter* **2014**, *26*, 284103.

(19) Maggs, A. C.; Podgornik, R. General Theory of Asymmetric Steric Interactions in Electrostatic Double Layers. *Soft Matter* **2016**, *12*, 1219–1229.

(20) Goodwin, Z. A. H.; Feng, G.; Kornyshev, A. A. Mean-Field Theory of Electrical Double Layer In Ionic Liquids with Account of Short-Range Correlations. *Electrochim. Acta* **2017**, *225*, 190–197.

(21) Aliaga, C.; Baldelli, S. Sum Frequency Generation Spectroscopy and Double-Layer Capacitance Studies of the 1-Butyl-3-Methylimidazolium Dicyanamide-Platinum Interface. *J. Phys. Chem. B* **2006**, *110*, 18481–18491.

(22) Kislenko, S. A.; Samoylov, I. S.; Amirov, R. H. Molecular Dynamics Simulation of the Electrochemical Interface Between a Graphite Surface and the Ionic Liquid [BMIM][PF$_6$]. *Phys. Chem. Chem. Phys.* **2009**, *11*, 5584–5590.

(23) Wang, S.; Li, S.; Cao, Z.; Yan, T. Y. Molecular Dynamic Simulations of Ionic Liquids at Graphite Surface. *J Phys. Chem. C* **2010**, *114*, 990–995.

(24) Merlet, C.; Salanne, M.; Rotenberg, B.; Madden, P. A. Imidazolium Ionic Liquid Interfaces with Vapor and Graphite: Interfacial Tension and Capacitance from Coarse-Grained Molecular Simulations. *The Journal of Physical Chemistry C* **2011**, *115*, 16613–16618.

(25) Vatamanu, J.; Borodin, O.; Bedrov, D.; Smith, G. D. Molecular Dynamics Simulation Study of the Interfacial Structure and Differential Capacitance of Alkylimidazolium Bis(trifluoromethanesulfonyl)imide [Cnmim][TFSI] Ionic Liquids at Graphite Electrodes. *J. Phys. Chem. C* **2012**, *116*, 7940–7951.

(26) Hu, Z.; Vatamanu, J.; Borodin, O.; Bedrov, D. A Molecular Dynamics Simulation Study of the Electric Double Layer and Capacitance of [BMIM][PF$_6$] and [BMIM][BF$_4$] Room Temperature Ionic Liquids Near Charged Surfaces. *Phys. Chem. Chem. Phys.* **2013**, *15*, 14234–47.

(27) Li, H.; Endres, F.; Atkin, R. Effect of Alkyl Chain Length and Anion Species on the

Interfacial Nanostructure of Ionic Liquids at the Au(111)-Ionic Liquid Interface as a Function of Potential. *Phys. Chem. Chem. Phys.* **2013**, *15*, 14624–33.

(28) Perkin, S. Ionic Liquids in Confined Geometries. *Phys. Chem. Chem. Phys.* **2012**, *14*, 5052–5062.

(29) Hu, Z. Z.; Vatamanu, J.; Borodin, O.; Bedrov, D. A Comparative Study of Alkylimidazolium Room Temperature Ionic Liquids with FSI and TFSI Anions near Charged Electrodes. *Electrochim. Acta* **2014**, *145*, 40–52.

(30) Jo, S.; Park, S.-W.; Shim, Y.; Jung, Y. Effects of Alkyl Chain Length on Interfacial Structure and Differential Capacitance in Graphene Supercapacitors: A Molecular Dynamics Simulation Study. *Electrochim. Acta* **2017**, *247*, 634–645.

(31) Noh, C.; Jung, Y. Understanding the Charging Dynamics of an Ionic Liquid Electric Double Layer Capacitor via Molecular Dynamics Simulations. *Phys. Chem. Chem. Phys.* **2019**, *21*, 6790–6800.

(32) Sha, M.; Wu, G.; Dou, Q.; Tang, Z.; Fang, H. Double-Layer Formation of [Bmim][PF_6] Ionic Liquid Triggered by Surface Negative Charge. *Langmuir* **2010**, *26*, 12667–72.

(33) Merlet, C.; Rotenberg, B.; Madden, P. A.; Salanne, M. Computer Simulations Of Ionic Liquids At Electrochemical Interfaces. *Phys. Chem. Chem. Phys.* **2013**, *15*, 15781–92.

(34) Feng, G.; Zhang, J. S.; Qiao, R. Microstructure and Capacitance of the Electrical Double Layers at the Interface of Ionic Liquids and Planar Electrodes. *J Phys Chem C* **2009**, *113*, 4549–4559.

(35) Nishi, N.; Hirano, Y.; Motokawa, T.; Kakiuchi, T. Ultraslow Relaxation of the Structure at the Ionic Liquid—Gold Electrode Interface to a Potential Step Probed by Electrochemical Surface Plasmon Resonance Measurements: Asymmetry of the Relaxation

Time to the Potential-Step Direction. *Phys. Chem. Chem. Phys.* **2013**, *15*, 11615–11619.

(36) Nishi, N.; Uruga, T.; Tanida, H. Potential Dependent Structure of an Ionic Liquid at Ionic Liquid/Water Interface Probed by X-Ray Reflectivity Measurements. *J. Electroanal. Chem.* **2015**, *759*, 129–136.

(37) Nishi, N.; Minami, K.; Motobayashi, K.; Osawa, M.; Sakka, T. Interfacial Structure at the Quaternary Ammonium-Based Ionic Liquids—Gold Electrode Interface Probed by Surface-Enhanced Infrared Absorption Spectroscopy: Anion Dependence of the Cationic Behavior. *J. Phys. Chem. C* **2017**, *121*, 1658–1666.

(38) Nishi, N.; Ikeda, Y.; Sakka, T. Electrochemical Surface Plasmon Resonance as a Probe of Redox Reactions at the Ionic Liquid—Gold Interface. *J. Electroanal. Chem.* **2018**, *817*, 210–216.

(39) Duarte, D.; Salanne, M.; Rotenberg, B.; Bizeto, M. A.; Siqueira, L. J. Structure of Tetraalkylammonium Ionic Liquids in the Interlayer of Modified Montmorillonite. *J Phys. Condens. Matter* **2014**, *26*, 284107.

(40) Sharma, S.; Kashyap, H. K. Structure of Quaternary Ammonium Ionic Liquids at Interfaces: Effects of Cation Tail Modification with Isoelectronic Groups. *J. Phys. Chem. C* **2015**, *119*, 23955–23967.

(41) Katakura, S.; Nishi, N.; Kobayashi, K.; Amano, K.-i.; Sakka, T. An Electric Double Layer Structure and Differential Capacitance at the Electrode Interface of Tributylmethylammonium Bis(trifluoromethanesulfonyl)amide Studied Using a Molecular Dynamics Simulation. *Phys. Chem. Chem. Phys.* **2020**, *22*, 5198–5210.

(42) Mousavi, M. P. S.; Kashefolgheta, S.; Stein, A.; Bühlmann, P. Electrochemical Stability of Quaternary Ammonium Cations: An Experimental and Computational Study. *J. Electrochem. Soc.* **2016**, *163*, H74–H80.

(43) Sato, T.; Masuda, G.; Takagi, K. Electrochemical Properties of Novel Ionic Liquids for Electric Double Layer Capacitor Applications. *Electrochim. Acta* **2004**, *49*, 3603–3611.

(44) Sharma, S.; Kashyap, H. K. Interfacial Structure of Pyrrolidinium Cation Based Ionic Liquids at Charged Carbon Electrodes: The Role of Linear and Nonlinear Alkyl Tails. *J. Phys. Chem. C* **2017**, *121*, 13202–13210.

(45) Sharma, S.; Dhattarwal, H. S.; Kashyap, H. K. Molecular Dynamics Investigation of Electrostatic Properties of Pyrrolidinium Cation Based Ionic Liquids near Electrified Carbon Electrodes. *J. Mol. Liq.* **2019**, *291*, 111269.

(46) Katakura, S.; Nishi, N.; Kobayashi, K.; Amano, K.; Sakka, T. Surface Structure of Quaternary Ammonium-Based Ionic Liquids Studied Using Molecular Dynamics Simulation: Effect of Switching the Length of Alkyl Chains. *J. Phys. Chem. C* **2019**, *123*, 7246–7258.

(47) Smith, W.; Forester, T. R. DL_POLY_2.0: A General-Purpose Parallel Molecular Dynamics Simulation Package. *J. Mol. Graph.* **1996**, *14*, 136–141.

(48) Canongia Lopes, J. N.; Pádua, A. A. H. Molecular Force Field for Ionic Liquids Composed of Triflate or Bistriflylimide Anions. *J. Phys. Chem. B* **2004**, *108*, 16893–16898.

(49) Rizzo, R. C.; Jorgensen, W. L. OPLS All-Atom Model for Amines: Resolution of the Amine Hydration Problem. *J. Am. Chem. Soc.* **1999**, *121*, 4827–4836.

(50) Chaban, V. Polarizability Versus Mobility: Atomistic Force Field for Ionic Liquids. *Phys. Chem. Chem. Phys.* **2011**, *13*, 16055–16062.

(51) Leontyev, I.; Stuchebrukhov, A. Accounting for Electronic Polarization in Nonpolarizable Force Fields. *Phys. Chem. Chem. Phys.* **2011**, *13*, 2613–26.

(52) Schröder, C. Comparing Reduced Partial Charge Models with Polarizable Simulations of Ionic Liquids. *Phys. Chem. Chem. Phys.* **2012**, *14*, 3089–102.

(53) Bhattacharjee, A.; Luís, A.; Santos, J. H.; Lopes-da Silva, J. A.; Freire, M. G.; Carvalho, P. J.; Coutinho, J. A. P. Thermophysical Properties of Sulfonium- and Ammonium-Based Ionic Liquids. *Fluid Phase Equilib.* **2014**, *381*, 36–45.

(54) Nishi, N.; Kasuya, K.; Kakiuchi, T. Surface Structure of a Hydrophobic Ionic Liquid Probed by Spectroscopic Ellipsometry. *J. Phys. Chem. C* **2012**, *116*, 5097–5102.

(55) Berendsen, H. J. C.; Postma, J. P. M.; van Gunsteren, W. F.; DiNola, A.; Haak, J. R. Molecular-Dynamics with Coupling to an External Bath. *J. Chem. Phys.* **1984**, *81*, 3684–3690.

(56) Essmann, U.; Perera, L.; Berkowitz, M. L.; Darden, T.; Lee, H.; Pedersen, L. G. A Smooth Particle Mesh Ewald Method. *J. Chem. Phys.* **1995**, *103*, 8577–8593.

(57) Ivaništšev, V.; Kirchner, K.; Kirchner, T.; Fedorov, M. V. Restructuring of the Electrical Double Layer in Ionic Liquids upon Charging. *J. Phys. Condens. Matter* **2015**, *27*, 102101.

(58) Kislenko, S. A.; Amirov, R. H.; Samoylov, I. S. Molecular Dynamics Simulation of the Electrical Double Layer in Ionic Liquids. *J Phys. Conf. Ser.* **2013**, *418*, 012021.

(59) Wen, R.; Rahn, B.; Magnussen, O. M. Potential-Dependent Adlayer Structure and Dynamics at the Ionic Liquid/Au(111) Interface: A Molecular-Scale In Situ Video-STM Study. *Angew. Chem. Int. Ed. Engl.* **2015**, *54*, 6062–6066.

(60) Nishi, N.; Hashimoto, A.; Minami, E.; Sakka, T. Electrocapillarity and Zero-Frequency Differential Capacitance at the Interface Between Mercury and Ionic Liquids Measured Using the Pendant Drop Method. *Phys. Chem. Chem. Phys.* **2015**, *17*, 5219–5226.

(61) Haskins, J. B.; Lawson, J. W. Evaluation of Molecular Dynamics Simulation Methods for Ionic Liquid Electric Double Layers. *J. Chem. Phys.* **2016**, *144*, 184707.

(62) Vatamanu, J.; Borodin, O.; Smith, G. D. Molecular Simulations of the Electric Double Layer Structure, Differential Capacitance, and Charging Kinetics for N-methyl-N-propylpyrrolidinium Bis(fluorosulfonyl)imide at Graphite Electrodes. *J. Phys. Chem. B* **2011**, *115*, 3073–84.

(63) Nishi, N.; Uchiyashiki, J.; Oogami, R.; Sakka, T. Ionic Liquid Structure at the Electrified Ionic Liquid|Hg Interface Studied Using In Situ Spectroscopic Ellipsometry. *Thin Solid Films* **2014**, *571*, 735–738.

Graphical TOC Entry